

# Highly Stretchable Carbon Nanotubes/Polymer Thermoelectric Fibers

Chunyang Zhang,<sup>‡</sup> Quan Zhang,<sup>‡</sup> Ding Zhang, Mengyan Wang, Yiwen Bo, Xiangqian Fan, Fengchao Li, Jiajie Liang, Yi Huang, Rujun Ma,<sup>\*</sup> and Yongsheng Chen

Cite This: *Nano Lett.* 2021, 21, 1047–1055

Read Online

ACCESS |

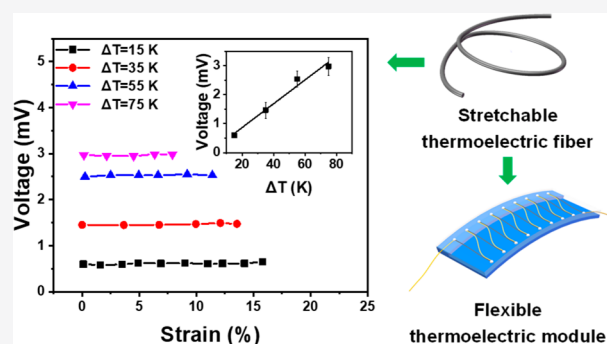
Metrics & More

Article Recommendations

Supporting Information

**ABSTRACT:** Thermoelectric (TE) technology provides a new way to directly harvest and convert the heat continuously released from the human body. The greatest challenge for TE materials applied in wearable TE generators is compatible with the constantly changing morphology of the human body while offering a continuous and stable power output. Here, a stretchable carboxylic single-walled carbon nanotube (SWNT)-based TE fiber is prepared by an improved wet-spinning method. The stable Seebeck coefficient of the annealed carboxylic SWNT-based TE fiber is 44  $\mu\text{V}/\text{K}$  even under the tensile strain of  $\sim 30\%$ . Experimental results show that the fiber can continue to generate constant TE potential when it is changed to various shapes. The new stretchable TE fiber has a larger Seebeck coefficient and more stretchability than existing TE fibers based on the Seebeck effect, opening a path to using the technology for a variety of practical applications.

**KEYWORDS:** Carbon nanotubes, Thermoelectric materials, Seebeck effect, Stretchable fibers



Since its discovery, thermoelectric (TE) technology based on the Seebeck effect has provided a unique method to directly convert heat to electrical energy without causing environmental pollution.<sup>1–4</sup> For this kind of TE generator, the maximum electric potential that can be generated mainly depends on the energy conversion efficiency of the TE material and actual temperature difference between the hot and the cool ends. The human body, like a continuous constant temperature source, has the potential to provide an inexhaustible energy, if the heat loss can be collected and converted effectively.<sup>5</sup> The electricity generated by the huge population on the earth is quite considerable. It can be directly used to drive the wearable electronics operation and even collected to make up the shortfall in demand for electricity. Therefore, more and more studies have focused on wearable TE materials for the human body.<sup>6,7</sup>

In order to meet the requirements of wearability, TE materials must have good mechanical flexibility and preferably stretchability.<sup>5,6,8</sup> Inorganic TE materials with a high Seebeck coefficient have an outstanding TE performance.<sup>1–3</sup> The biggest challenge for them in the application of wearable TE generators is that it is difficult to match the body whose morphology changes with human motion. A common method is to coat inorganic TE materials on various flexible substrates (such as polymer film and fiber) by vacuum filtration,<sup>9,10</sup> spin-coating,<sup>11</sup> drop-casting,<sup>12–15</sup> blade-coating,<sup>16</sup> printing,<sup>17,18</sup> and physical and chemical vapor deposition.<sup>19,20</sup> To avoid the

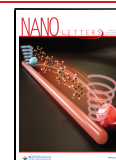
fracture of TE materials, the devices with layer structure or core–shell structure can only be bent, even if the substrate is stretchable. Another design is to integrate bulk TE legs into an elastic polymer connected with stretchable electrodes.<sup>21,22</sup> In this way, the final TE generator is stretchable; however, it is not suitable for covering a larger area of the human body due to its impermeability.

Conductive polymers are a class of promising TE materials because of their mechanical flexibility. Among them, poly(3,4-ethylenedioxythiophene) polystyrenesulfonate (PEDOT:PSS) has the highest energy conversion efficiency and thus attracts more attention to application in flexible TE generators.<sup>23</sup> Compared with inorganic TE materials, the low Seebeck coefficient limits the TE performance of PEDOT:PSS. In some studies, inorganic TE materials with a high Seebeck coefficient or high conductivity are mixed into PEDOT:PSS to improve the TE performance of the composite, but this leads to a decrease in flexibility and stretchability.<sup>14,24–27</sup> Carbon materials, including carbon nanotubes (CNTs) and graphene, are flexible and conductive due to the characteristic structure

Received: October 27, 2020

Revised: January 1, 2021

Published: January 6, 2021



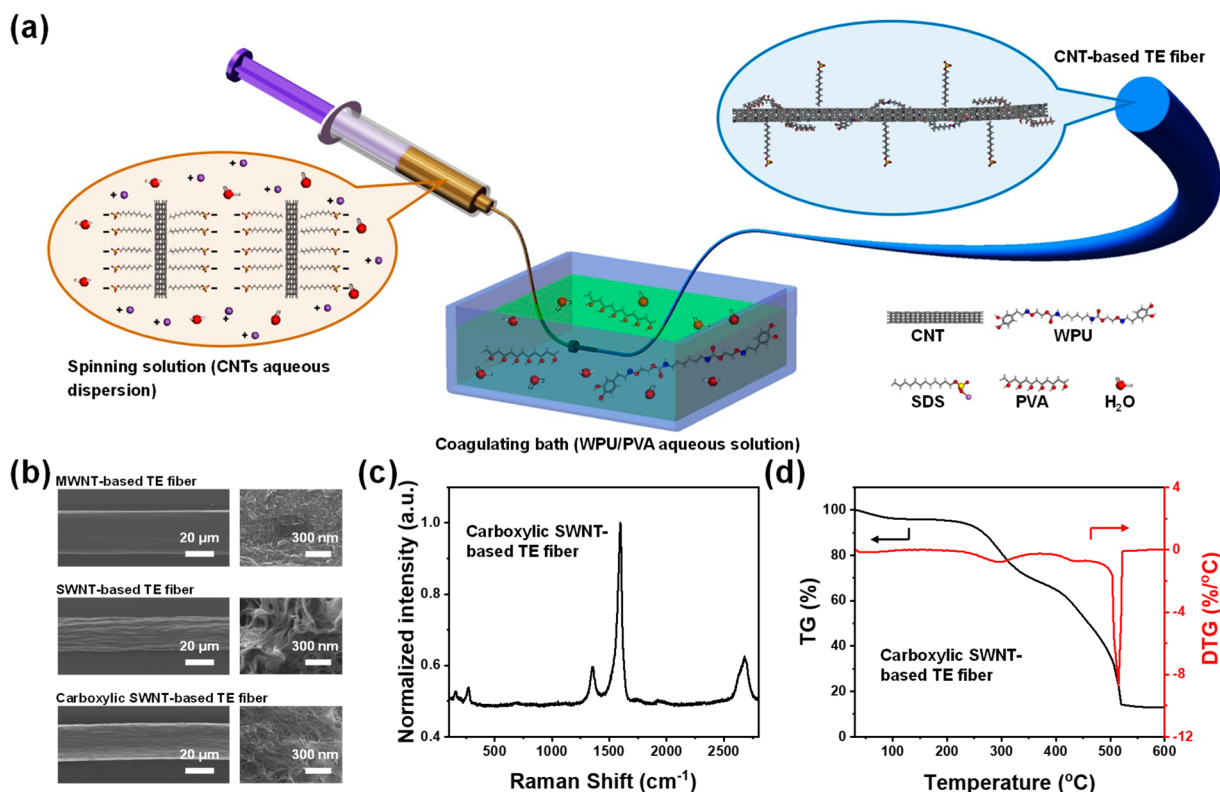


**Figure 1.** Synthesis of CNT-based TE fibers. (a) Schematic illustration of the experimental setup used to fabricate CNT-based composite TE fibers. (b) Morphology (left) and cross-sectional (right) SEM images of the carboxylic SWNT-based fiber, MWNT-based fiber, and SWNT-based fiber. (c) Raman spectroscopy of the carboxylic SWNT-based fiber at an excitation wavelength of 532 nm. (d) TGA and DTG of carboxylic SWNT-based composite TE fiber under 20 vol % O<sub>2</sub> and 80 vol % Ar.

of the two-dimensional hexagonal lattice of carbon atoms.<sup>28–32</sup> The strong  $\pi$ – $\pi$  interaction between CNTs (or graphene) and PEDOT:PSS can effectively improve the conductivity of the composite while maintaining its flexibility.<sup>5,33–38</sup> In addition to conductive polymers, graphene can also be solely mixed into the elastomer to prepare flexible TE materials.<sup>39–42</sup> The resistance of some graphene-based TE materials is generally sensitive to mechanical strain. Thus, they are more suitable for TE sensors rather than TE generators.<sup>43,44</sup> However, most current wearable TE materials are only flexible rather than intrinsically stretchable. Their maximum tensile strain is usually less than 10%, which cannot satisfy the actual demand for wearable TE devices.<sup>45,46</sup> Therefore, it is quite necessary to develop new stretchable TE materials.

Here, we reported a stretchable CNT-based TE fiber fabricated by improved wet-spinning technology. The optimized carboxylic single-walled carbon nanotube (SWNT)-based TE fiber had a Seebeck coefficient of 44.0  $\mu\text{V}/\text{K}$  under the tensile strain of  $\sim 30\%$ . The experimental results showed that the resistance change ratio of the TE fiber was only 10% under a tensile strain of 20%, and the maximum output power was about 400 pW under the temperature difference of 50 K. There was no obvious change in the open-circuit voltage of the TE fiber when it was stretched or bent. Further, a wearable and compact TE device was integrated using optimized carboxylic SWNT-based TE fibers. The device can conform to surfaces with complex curvature and also operates with excellent performance.

CNT-based TE fibers are prepared by an improved wet-spinning method (Figure 1a).<sup>47</sup> CNT powders are well dispersed in deionized water by probe ultrasonication as the

spinning solution, where sodium dodecyl sulfate (SDS) is used as the surfactant to avoid aggregation of CNTs. A mixed aqueous solution containing 5 wt % waterborne polyurethane (WPU) and 5 wt % poly(vinyl alcohol) (PVA) is used as a coagulating bath. Then, the CNT-based spinning solution is gradually extruded into the coagulation bath through a syringe needle with a diameter of 300  $\mu\text{m}$ . Meanwhile, the needle moves slowly along the opposite direction of spinning solution outflow. In this way, a fiber is left and *in situ* immersed in the coagulation bath for 10 min. During this period, the water in the spinning solution is extracted out. Meanwhile, different from the general wet-spinning process,<sup>48</sup> WPU and PVA molecular chains in the coagulating bath reversely infiltrate into the gap between adjacent CNTs, due to the concentration gradient between the spinning solution and the coagulation bath. After that, the fiber is repeated to transfer and immerse in deionized water several times to remove redundant WPU, PVA, and SDS. After natural drying in air, the as-prepared CNT-based TE fibers are annealed in vacuum to improve their mechanical properties and TE performance.

Figure 1b shows the morphology of TE fibers prepared by three kinds of different CNTs. The TE fibers prepared by multiwalled carbon nanotubes (MWNTs) and carboxylic SWNTs are both cylindrical, while the SWNT-based TE fiber is a flat strip. This may be related to the dispersed state of the CNTs in the spinning solution. Compared with MWNTs and carboxylic SWNTs, it is difficult to monodisperse SWNTs in deionized water only with SDS because of the strong intermolecular interaction between SWNTs.<sup>49,50</sup> From the cross-sectional scanning electron microscope (SEM) images, SWNTs exist in the fiber in the form of a bundle, and MWNTs

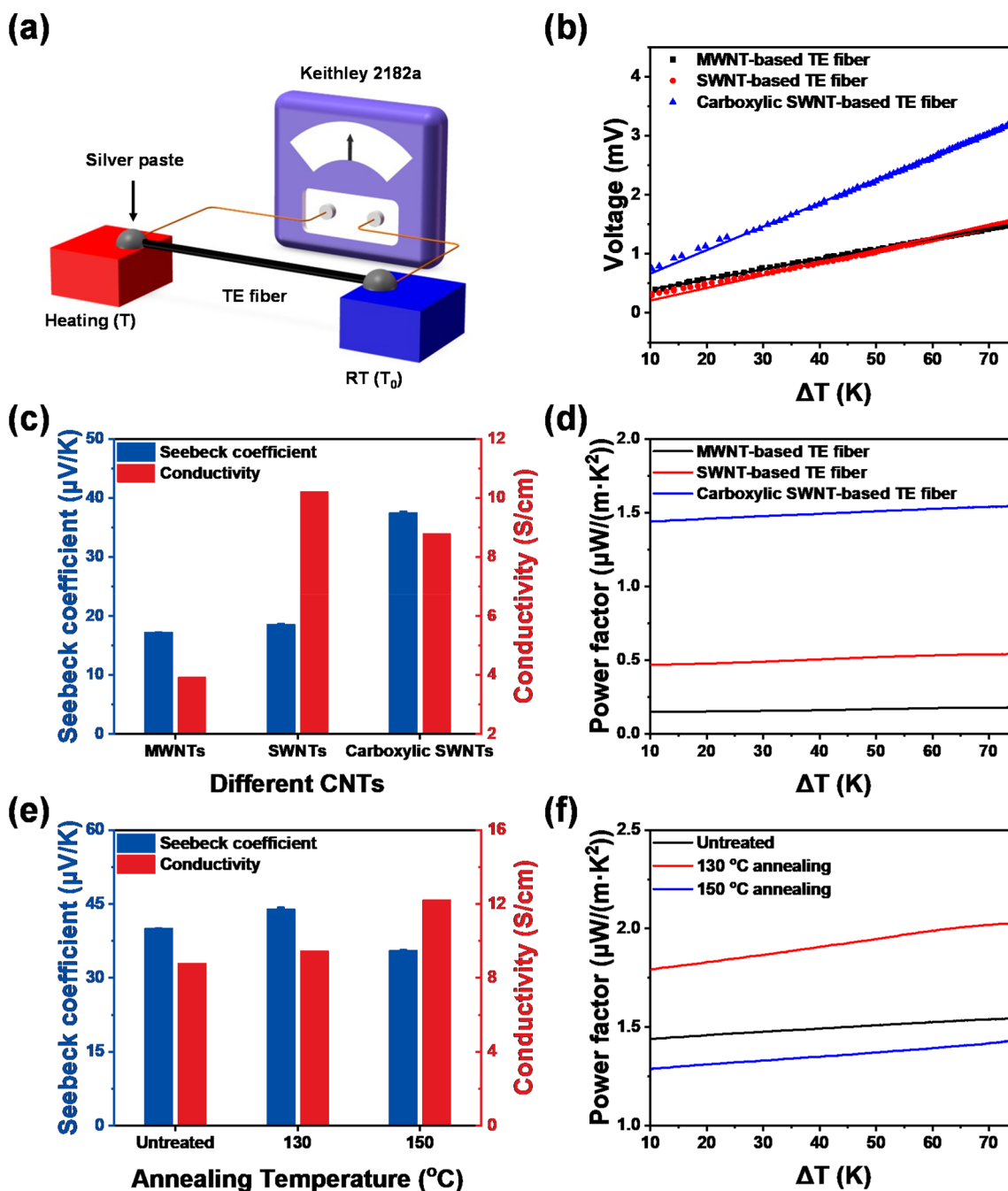


**Figure 2.** TE performance of CNT-based TE fibers. (a) Schematic illustration of the measurement setup for the open-circuit voltage of the TE fiber. (b) Open-circuit voltage of the TE fiber prepared by three kinds of CNTs as a function of the temperature difference between the hot and the cool ends ( $\Delta T = T - T_0$ ). The line with the same color is the corresponding fitting result. (c) Seebeck coefficient and conductivity at RT of the fibers prepared with three kinds of CNTs. (d) Power factor of the TE fibers prepared with three kinds of CNTs as a function of temperature difference ( $\Delta T$ ). (e) Seebeck coefficient and conductivity at RT of the fibers annealed at different temperatures. (f) Power factor of the TE fibers annealed at different temperatures as a function of temperature difference ( $\Delta T$ ).

and carboxylic SWNTs uniformly distribute in the fibers. As shown in Figure S1, the fiber with the length of 350 mm was collected on a metal rod, and the diameter of the fiber was uniform ( $\sim 26 \mu\text{m}$ ).

The high concentration of the WPU-PVA aqueous solution as the coagulation bath does not only extract out water from the spinning solution but also provides an opportunity for polymer molecular chains to infiltrate into the gaps between the CNTs. As shown in the cross-sectional SEM images, the CNTs in the three kinds of fibers are all wrapped by a polymer

(Figure 1b). The characteristic peaks in Raman spectroscopy indicate the presence of carboxylic SWNTs in the TE fiber (Figure 1c). The carboxylic SWNT-based fibers are further characterized by thermal gravimetric analysis (TGA). As the temperature increases, the fiber gradually decomposes in a mixed atmosphere containing 20 vol % oxygen ( $\text{O}_2$ ) and 80 vol % argon (Ar). Compared with TGA curves of each individual component in the fiber, it can be determined that the fiber is composed of carboxylic SWNT, SDS, PVA, and WPU according to the characteristic peaks in the differential thermal

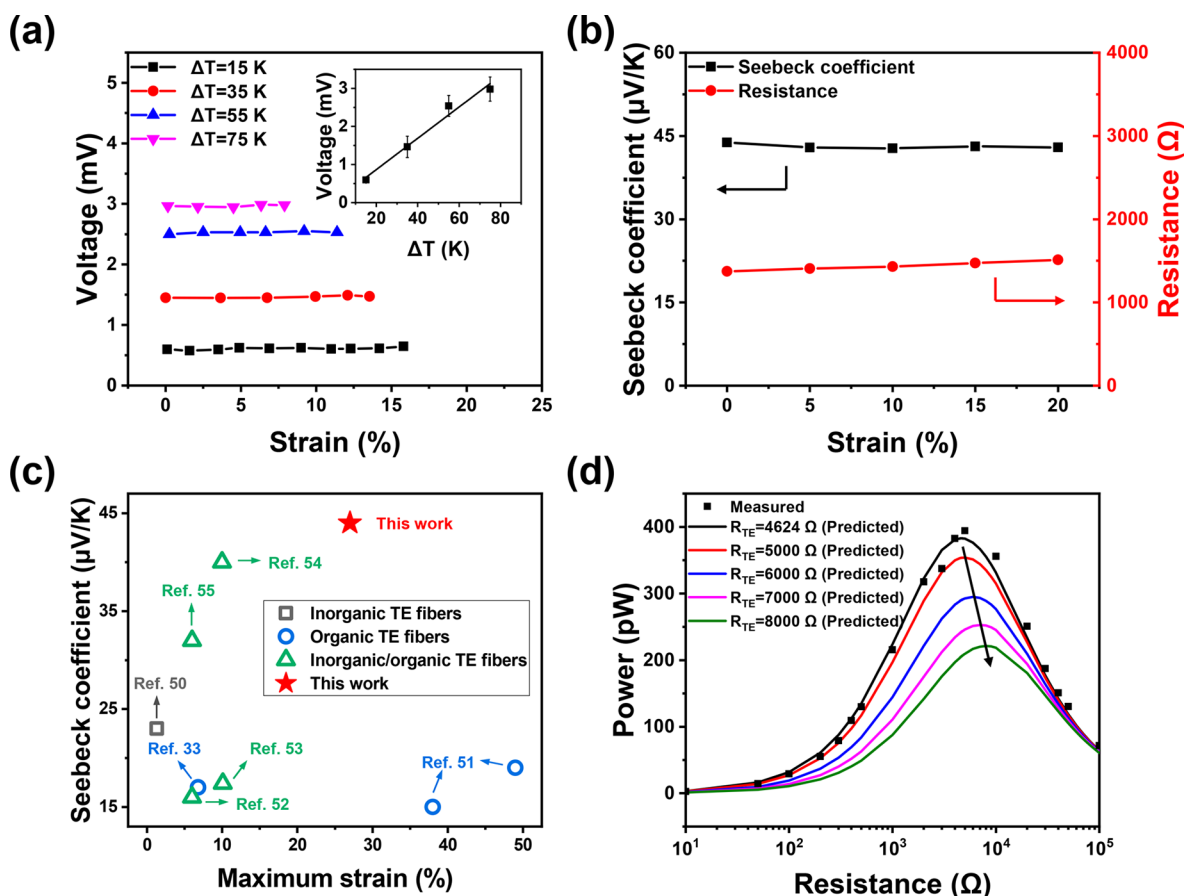


**Figure 3.** TE performance of the carboxylic SWNT-based fiber under the tensile state. (a) Open-circuit voltage of an individual carboxylic SWNT-based fiber with different strains and hot end temperatures. The voltage gradually improves with the increase of the hot end temperature. The inset shows that the average voltage has a linear correlation with a temperature difference between hot and cool ends. (b) Seebeck coefficient and resistance of an individual carboxylic SWNT-based fiber under different strains. (c) Maximum strain with the corresponding Seebeck coefficient of the carboxylic SWNT-based TE fiber is compared with those of control stretchable TE fibers in the literature. (d) Measured (square) and predicted (line) output powers of an individual carboxylic SWNT-based fiber in terms of the external load resistance.

gravimetric (DTG) curves (Figure 1d and Figure S2). The broad peaks at 298 and 436 °C are both the overlap results of SDS, PVA, and WPU. The peak at 515 °C is the typical characteristic peak of carboxylic SWNTs. When the temperature is higher than 550 °C, the residual weight is from the decomposition products of SDS. However, the above results indicate that the CNT-based TE fiber is a composite, which is made of pristine CNTs and SDS, and the infiltrated PVA and WPU.

To investigate the TE performance of the CNT-based TE fiber, a homemade measurement setup is installed as shown in Figure 2a. In order to ensure the uniform surface temperature, the copper (Cu) plates are attached to the surfaces of the hot and cool ends. A K-type thermocouple is used to measure the surface temperature of each end. A polyimide (PI) heater connected with an adjustable power supply is stuck on the back of the Cu plate to control the temperature at the heating end. The fiber is fixed by silver paste and connected with a voltmeter (Keithley 2182A) to record real-time dynamic data. During the experiment, the room temperature (RT) is always  $\sim 25$  °C. There is a linear relationship between the open-circuit voltage of the TE fiber and the temperature difference ( $\Delta T$ ) between the hot ( $T$ ) and the cool ( $T_0$ ) ends (Figure 2b and Figure S3). With increasing  $\Delta T$ , the open-circuit voltage gradually increases. The Seebeck coefficient is equal to the

slope of the relationship between the open-circuit voltage and the temperature difference, which is almost unchanged in the tested temperature range. Compared with TE fibers composed of MWNTs and SWNTs, the carboxylic SWNT-based TE fiber has a larger Seebeck coefficient (37.5  $\mu\text{V/K}$ ) and a higher open-circuit voltage under the same  $\Delta T$  (Figure 2c). Although the conductivity of the carboxylic SWNT-based TE fiber is slightly lower than that of the SWNT-based TE fiber, the calculated TE power factor shows that the carboxylic SWNT-based fiber has a better TE performance compared with the other two kinds of TE fibers. As the temperature at the hot end increases, the TE power factor also increases (Figure 2d).

The concentration of the spinning solution also affects the TE performance of the CNT-based fibers. We compared the TE performance of carboxylic SWNT-based fibers prepared by a spinning solution with different mass fractions of CNTs. As shown in Figure S4a, there is no significant change in the Seebeck coefficient of the TE fiber with increasing content of CNTs. The electrical conductivity of these TE fibers gradually improves with the increase of the hot end temperature (Figure S5). Among them, the TE fiber prepared by a spinning solution with 0.6 wt % carboxylic SWNTs has the highest conductivity. When the concentration of the spinning solution is larger than 0.6 wt %, the dispersed state of the carboxylic SWNTs in the solution degrades, thereby decreasing the

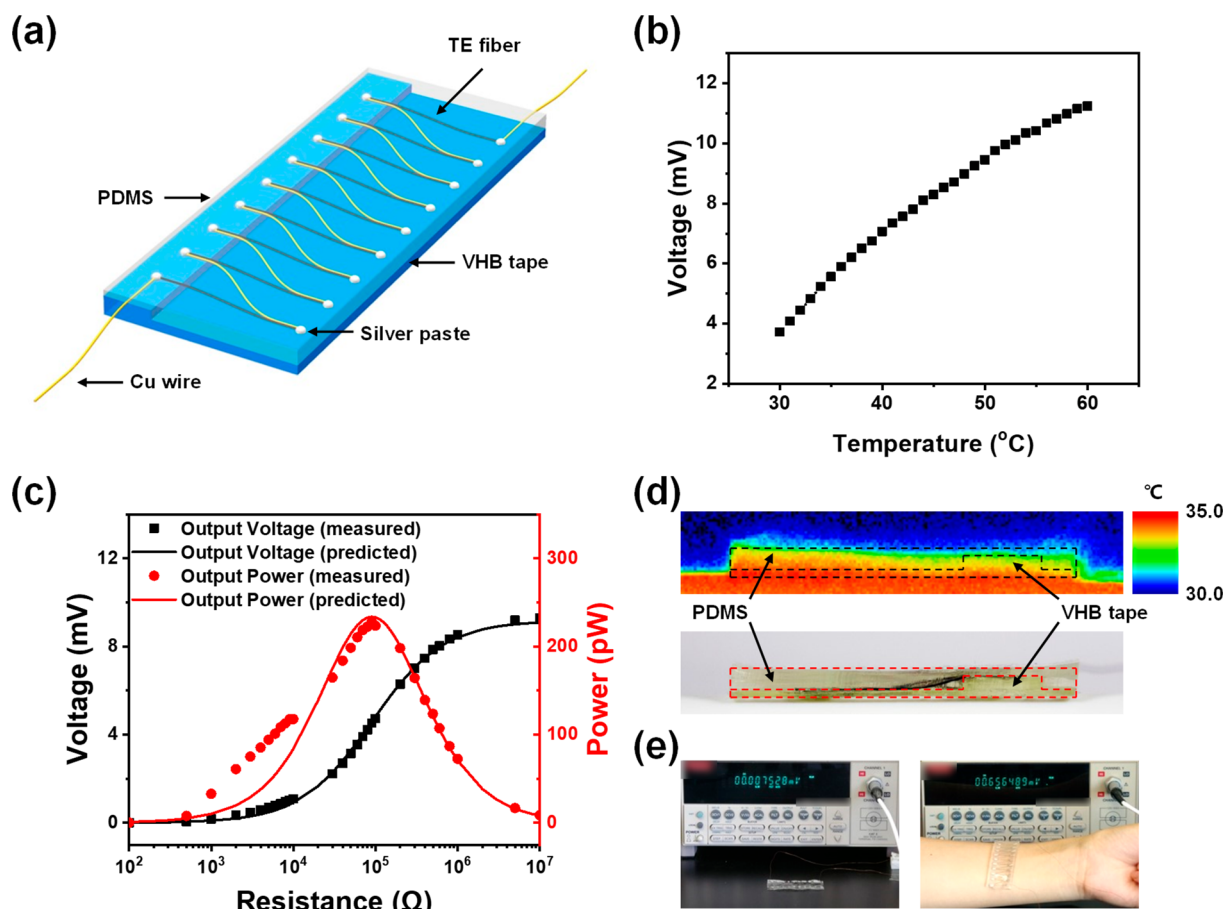


**Figure 4.** TE performance of a flexible device integrated by TE fibers. (a) Schematic illustration of a TE device. (b) Open-circuit voltage of the TE device at different temperatures of the hot end. (c) Measured and predicted output voltage and power of the TE device as a function of external load resistance. (d) Cross-sectional infrared and optical image of the TE device. (e) Change in open-circuit voltage of the TE device before (left) and after (right) being placed on the forearm.

conductivity of the fiber. There is no doubt that the fiber prepared by the spinning solution with 0.6 wt % carboxylic SWNTs has the highest TE power factor and it increases with the increase of  $\Delta T$  (Figure S4b).

Annealing treatment can further improve the TE performance of the carboxylic SWNT-based fiber. As the annealing temperature increases, the electrical conductivity of the fiber increases gradually. Meanwhile, the Seebeck coefficient increases first and then decreases (Figure 2e). According to the calculated TE power factor, TE fiber annealing at 130 °C shows the best power factor (Figure 2f). In general, the TE fiber annealed at 130 °C (0.6 wt % carboxylic SWNTs) exhibits the desired TE performance with the Seebeck coefficient of 44.0  $\mu\text{V}/\text{K}$  and power factor of 1.78  $\mu\text{W}/(\text{m}\cdot\text{K}^2)$  at RT.

To be wearable, the carboxylic SWNT-based TE fiber must meet the requirements for stretching. The fiber prepared from the WPU–PVA blended aqueous solution exhibits good stretchability. Compared with the fiber fabricated by a pure PVA aqueous solution, the introduction of WPU effectively enhances the stretchability of the TE fiber while reducing the elastic modulus (Figure S6). Considering both the TE performance and the mechanical properties, the TE fiber annealed at 130 °C (0.6 wt % carboxylic SWNTs) is used to further analyze the TE performance during stretching. Figure 3a shows that open-circuit voltage of the fiber does not change with the tensile strain, and it improves with the increase of  $\Delta T$ .

As shown in the inset in Figure 3a, the average voltage shows a near-linear relationship with the temperature difference. Figure 3b summarizes the Seebeck coefficient and resistance at RT of the TE fibers under different tensile strains. With increasing tensile strain, the Seebeck coefficient is almost unchanged and the electrical resistance of the TE fiber increases slightly. These results show that the resistance change of the fiber during stretching has little effect on the open-circuit voltage, which is mainly determined by the temperature difference between the hot and the cool ends. Whether the fiber is stretched or not, the Seebeck coefficient is always constant. It is worth noting that the maximum strain gradually decreases with the increasing temperature at the hot end. The TE performances of the fibers were compared undergoing different deformation states, such as stretching, bending, and twisting. Compared with the as-prepared fiber, there is only slight attenuation of the Seebeck coefficient and conductivity, when the TE fibers undergo 100 times stretching of 5% strain, 1000 times bending of 180°, and 1000 times twisting of 180°, respectively (Figure S7).

In order to further explore the TE fiber used in wearable applications, we investigated the effect of the humidity on the TE performance of the fiber (Figure S8). As a demonstration of practical application scenarios, the TE fibers exhibit good TE performance stability even if they are immersed in deionized (DI) water or synthetic perspiration for 1 h. It is worth noting that the conductivity increases slightly, when the

TE fiber is soaked in synthetic perspiration for 1 h. This may be caused by the existing free ions in synthetic perspiration. However, these results indicate that the sweating process (such as humidity) does not affect the TE performance of the fiber.

Figure 3c compares the Seebeck coefficient and maximum strain of the carboxylic SWNT-based TE fiber (filled symbol) with previously reported stretchable inorganic,<sup>51</sup> organic,<sup>33,52</sup> and inorganic/organic<sup>53–56</sup> TE fibers (open symbols) in the literature. The carboxylic SWNT-based TE fiber reaches a Seebeck coefficient of 44  $\mu\text{V}/\text{K}$  with a maximum tensile strain of  $\sim 30\%$ , setting a new mark for the stretchable TE fiber.

Furthermore, we measured the output voltage under  $\Delta T = 50\text{ K}$  for a variety of external load resistances (Figure 3d). It can be seen that the output voltage increases with the external load resistance. The output power increases first and then decreases with the external load resistance, and the maximum output power is  $\sim 394\text{ pW}$  corresponding to the external load resistance equal to the internal resistance of the fiber. We also estimated the output power ( $P$ ) by the following equation<sup>57</sup>

$$P = I^2 R_{\text{ex}} \quad (1)$$

where  $I$  is the current across the external load resistance and  $R_{\text{ex}}$  is the resistance of the external load. Because the measurement circuit can be simplified to a series circuit including external load resistance ( $R_{\text{ex}}$ ), the internal resistance of the TE fiber ( $R_{\text{TE}}$ ), circuit resistance ( $R_{\text{tot}}$ ), and a TE potential ( $U$ ), the current ( $I$ ) can be calculated by

$$I = \frac{U}{R_{\text{ex}} + R_{\text{TE}} + R_{\text{tot}}} \quad (2)$$

Based on the Seebeck effect, the total voltage is determined by the  $\Delta T$  between the hot and the cool ends.

$$U = \alpha \cdot \Delta T + U_0 \quad (3)$$

where  $\alpha$  is the Seebeck coefficient of the fiber and  $U_0$  is the intrinsic built-in electric potential at the contact interface between the TE fiber and the silver paste. As shown in Figure 3d, the measured output power (square) is consistent with the predicted value (line). The predicted results demonstrate that the maximum output power decreases toward the large external load resistance with the increase of the internal resistance of the TE fiber. For the carboxylic SWNT-based TE fiber, the experimental results have shown that the change in resistance of the fiber caused by stretching is negligible. Regardless of stretching, bending, or twisting, any human motions in practice do not have much effect on the output voltage of the carboxylic SWNT-based fiber (Figure S9). Figure S10 shows the output voltage under a lower temperature difference for a variety of external load resistances. In general, the temperature difference between the environment and the human body is usually less than 20 K. In this case, the maximum output power of an individual TE fiber increases from  $\sim 43\text{ pW}$  to  $\sim 80\text{ pW}$  with the increase of the temperature difference from 10 to 20 K.

Finally, we fabricated a wearable and compact TE device integrated by 10 TE fibers (Figure 4a). In the design, the fibers are placed on a VHB tape parallel along the axis at equal spacing. One side of each fiber is connected to the other side of the adjacent fiber by the Cu wire. The Cu wires connected to the ends of the outermost fibers are used as the output ends of the entire device. All the junctions are fixed with silver paste. A polydimethylsiloxane (PDMS) coating on all of the TE fibers

encapsulates the entire device. It is worth noting that one side of the fibers is raised up by a 1 mm-thick VHB tape. In this way, two asymmetric heat transfer paths are constructed artificially, due to the difference of thermal conductivity between the VHB tape and PDMS. When the device is placed on a flat heating source, there is a temperature difference between two ends due to the nonuniform heat transfer along the vertical direction. Among them, the end without a step is closer to the heat source, defined as the hot end.

A heating plate is used to control the temperature of the hot end alone. As shown in Figure 4b, the open-circuit voltage of the device increases with the increase of  $\Delta T$ . In this device, 10 fibers are connected in series. In theory, the open-circuit voltage of the device should be equal to the sum of the open-circuit voltages of each fiber. However, it is obviously lower than the open-circuit voltage of the 10 TE fibers in Figure 3a. The reason is that the actual temperature of the TE fiber at the hot end is lower than the heating temperature. Further, we measured the output voltage and power as a function of the external load resistance when the heating temperature of the hot end was  $55\text{ }^\circ\text{C}$  (Figure 4c). The output voltage gradually increases to the open-circuit voltage of this TE device with the external load resistance. The measured maximum output power is about 227.9 pW, when the external load resistance is equal to the resistance of the TE module. For the in-series circuit, the total voltage of the TE module is 10 times the voltage of an individual TE fiber. Based on this assumption, the predicted voltage and output power are both consistent with the measured results, while  $\Delta T$  is 10 K. The comparison between the predicted and the measured results shows that the temperature difference used in the prediction (10 K) is significantly lower than that in the experiment (30 K). It exactly verifies that the actual temperature of the TE fiber at the hot end is lower than that of the heating temperature.

Figure 4d shows the cross-sectional infrared image of a TE device placed on a heating plate at  $35\text{ }^\circ\text{C}$  and its cross-sectional morphology. The boundary between PDMS and the VHB tape has been marked with a dashed line. The infrared image shows a distinct temperature gradient along the vertical direction between the hot and the cool ends, which visually reveals the temperature difference between the ends of the TE fibers. The output voltage of the TE device placed on the desk was only  $7.5\text{ }\mu\text{V}$ . Once the device is placed on the forearm, the output voltage rapidly increases to 0.66 mV (Figure 4e). These results describe the great potential of the TE device integrated by a carboxylic SWNT-based fiber applied in the harvesting and conversion of human heat.

Figure S11 shows another two kinds of TE fiber-based TE textiles. One is TE fiber-based fabric, in which 20 TE fibers were woven into a fabric by a plain weave (Figure S11a). Along the longitude and latitude directions, 10 fibers are connected in parallel with each other, respectively. In this way, the total resistance of the fabric is lower than that of an individual TE fiber. The experimental results show that the output voltage of the TE fabric is 0.82 mV, basically equal to the output voltage of an individual TE fiber, when the temperature difference is 20 K. Thanks to the decrease in resistance, the maximum output power is 197 pW. Another way is to embroider the TE fiber into the cotton textile (Figure S11b). The TE fiber is periodically coated with silver paste, and the joints between the TE fiber and the silver paste-coated TE fiber are arranged on the two sides of the cotton textile alternately. The series of joints between the as-prepared TE fiber and the silver paste-

coated TE fiber raises the output voltage. When the cotton textile with the weaved TE fiber is placed on a 37 °C heating plate, the output voltage is 1.29 mV corresponding to the temperature difference of ~5 K at steady state (Figure S11c).

In conclusion, we fabricated a stretchable carboxylic SWNT-based TE fiber by an improved wet-spinning method. After annealing treatment, the fiber exhibits a stable Seebeck coefficient of 44.0  $\mu\text{V}/\text{K}$  and a maximum stretching strain of 27%. The experimental results show that the open-circuit voltage of the TE fiber is independent of the tensile strain, and the resistance increases by only 10% under the tensile strain of 20%. It indicates that fiber has the ability to provide a stable voltage output when it is changed into various shapes. Based on the above results, we designed a flexible TE device integrated with 10 TE fibers. When the device is attached on the skin surface, there is a stable voltage output of 0.66 mV. The moderate Seebeck coefficient, high tensile strain, and stable voltage output provide an opportunity for the application of carboxylic SWNT-based TE fibers in wearable TE generators.

## ■ ASSOCIATED CONTENT

### Supporting Information

The Supporting Information is available free of charge at <https://pubs.acs.org/doi/10.1021/acs.nanolett.0c04252>.

Details of materials, experimental methods, and characterization; TGA and DTG of different materials; TE performance of different TE fibers; mechanical properties of the carboxylic SWNT-based TE fiber; and open-circuit voltage of the TE fiber in the straight and bending states (PDF)

## ■ AUTHOR INFORMATION

### Corresponding Author

Rujun Ma – School of Materials Science and Engineering, National Institute for Advanced Materials, Tianjin Key Lab for Rare Earth Materials and Applications, Nankai University, Tianjin 300350, P. R. China; [orcid.org/0000-0001-7892-5212](https://orcid.org/0000-0001-7892-5212); Email: [malab@nankai.edu.cn](mailto:malab@nankai.edu.cn)

### Authors

Chunyang Zhang – School of Materials Science and Engineering, National Institute for Advanced Materials, Tianjin Key Lab for Rare Earth Materials and Applications, Nankai University, Tianjin 300350, P. R. China

Quan Zhang – School of Materials Science and Engineering, National Institute for Advanced Materials, Tianjin Key Lab for Rare Earth Materials and Applications, Nankai University, Tianjin 300350, P. R. China

Ding Zhang – School of Materials Science and Engineering, National Institute for Advanced Materials, Tianjin Key Lab for Rare Earth Materials and Applications, Nankai University, Tianjin 300350, P. R. China

Mengyan Wang – School of Materials Science and Engineering, National Institute for Advanced Materials, Tianjin Key Lab for Rare Earth Materials and Applications, Nankai University, Tianjin 300350, P. R. China

Yiwen Bo – School of Materials Science and Engineering, National Institute for Advanced Materials, Tianjin Key Lab for Rare Earth Materials and Applications, Nankai University, Tianjin 300350, P. R. China

Xiangqian Fan – School of Materials Science and Engineering, National Institute for Advanced Materials, Tianjin Key Lab for Rare Earth Materials and Applications, Nankai University, Tianjin 300350, P. R. China

Fengchao Li – School of Materials Science and Engineering, National Institute for Advanced Materials, Tianjin Key Lab for Rare Earth Materials and Applications, Nankai University, Tianjin 300350, P. R. China

Jiajie Liang – School of Materials Science and Engineering, National Institute for Advanced Materials, Tianjin Key Lab for Rare Earth Materials and Applications, Nankai University, Tianjin 300350, P. R. China; [orcid.org/0000-0003-2112-6721](https://orcid.org/0000-0003-2112-6721)

Yi Huang – School of Materials Science and Engineering, National Institute for Advanced Materials, Tianjin Key Lab for Rare Earth Materials and Applications, Nankai University, Tianjin 300350, P. R. China; [orcid.org/0000-0001-9343-207X](https://orcid.org/0000-0001-9343-207X)

Yongsheng Chen – State Key Laboratory and Institute of Elemento-Organic Chemistry, Centre of Nanoscale Science and Technology and Key Laboratory of Functional Polymer Materials, College of Chemistry, Nankai University, Tianjin 300071, P. R. China; [orcid.org/0000-0003-1448-8177](https://orcid.org/0000-0003-1448-8177)

Complete contact information is available at: <https://pubs.acs.org/doi/10.1021/acs.nanolett.0c04252>

### Author Contributions

\*(C.Z. and Q.Z.) These authors contributed equally.

### Notes

The authors declare no competing financial interest.

## ■ ACKNOWLEDGMENTS

This work is supported by National Key R&D Program of China (Grant No. 2020YFA0711500), the National Natural Science Fund of China (51973095, 52011540401, and 21421001), and “Fundamental Research Funds for the Central Universities”, Nankai University (023-92022018).

## ■ ABBREVIATIONS

TE, thermoelectric; SWNT, single-walled carbon nanotube; PEDOT:PSS, poly(3,4-ethylenedioxythiophene) polystyrene-sulfonate; CNTs, carbon nanotubes; SDS, sodium dodecyl sulfate; WPU, waterborne polyurethane; PVA, poly(vinyl alcohol); MWNT, multiwalled carbon nanotube; SEM, scanning electron microscope; TGA, thermal gravimetric analysis; O<sub>2</sub>, oxygen; Ar, argon; DTG, differential gravimetric; Cu, copper; PI, polyimide; RT, room temperature

## ■ REFERENCES

- (1) Chang, C.; Wu, M.; He, D.; Pei, Y.; Wu, C.; Wu, X.; Yu, H.; Zhu, F.; Wang, K.; Chen, Y.; Huang, L.; Li, J.; He, J.; Zhao, L. 3D charge and 2D phonon transports leading to high out-of-plane ZT in n-type SnSe crystals. *Science* **2018**, *360* (6390), 778–783.
- (2) He, W.; Wang, D.; Wu, H.; Xiao, Y.; Zhang, Y.; He, D.; Feng, Y.; Hao, Y.; Dong, J.; Chetty, R.; Hao, L.; Chen, D.; Qin, J.; Yang, Q.; Li, X.; Song, J.; Zhu, Y.; Xu, W.; Niu, C.; Li, X.; Wang, G.; Liu, C.; Ohta, M.; Pennycook, S. J.; He, J.; Li, J.; Zhao, L. High thermoelectric performance in low-cost Sn<sub>50</sub>Se<sub>0.09</sub> crystals. *Science* **2019**, *365* (6460), 1418–1424.
- (3) Zhao, L.; Tan, G.; Hao, S.; He, J.; Pei, Y.; Chi, H.; Wang, H.; Gong, S.; Xu, H.; Dravid, V. P.; Uher, C.; Snyder, G. J.; Wolverton, C.; Kanatzidis, M. G. Ultrahigh power factor and thermoelectric

performance in hole-doped single-crystal SnSe. *Science* **2016**, *351* (6269), 141–144.

(4) Liu, Z.; Chen, G. Advancing Flexible Thermoelectric Devices with Polymer Composites. *Adv. Mater. Technol.* **2020**, *5* (7), 2000049.

(5) Huang, L.; Lin, S.; Xu, Z.; Zhou, H.; Duan, J.; Hu, B.; Zhou, J. Fiber-Based Energy Conversion Devices for Human-Body Energy Harvesting. *Adv. Mater.* **2020**, *32* (5), 1902034.

(6) Wang, Y.; Yang, L.; Shi, X. L.; Shi, X.; Chen, L.; Dargusch, M. S.; Zou, J.; Chen, Z. G. Flexible Thermoelectric Materials and Generators: Challenges and Innovations. *Adv. Mater.* **2019**, *31* (29), 1807916.

(7) Yamamoto, N.; Takai, H. Electrical power generation from a knitted wire panel using the thermoelectric effect. *Electr. Eng. Jpn.* **2002**, *140* (1), 16–21.

(8) Zhang, D.; Wang, Y.; Yang, Y. Design, Performance, and Application of Thermoelectric Nanogenerators. *Small* **2019**, *15* (32), 1805241.

(9) Wu, B.; Guo, Y.; Hou, C.; Zhang, Q.; Li, Y.; Wang, H. High-Performance Flexible Thermoelectric Devices Based on All-Inorganic Hybrid Films for Harvesting Low-Grade Heat. *Adv. Funct. Mater.* **2019**, *29* (25), 1900304.

(10) Zhou, Y.; Wan, J.; Li, Q.; Chen, L.; Zhou, J.; Wang, H.; He, D.; Li, X.; Yang, Y.; Huang, H. Chemical Welding on Semimetallic TiS<sub>2</sub> Nanosheets for High-Performance Flexible n-Type Thermoelectric Films. *ACS Appl. Mater. Interfaces* **2017**, *9* (49), 42430–42437.

(11) Choi, J.; Cho, K.; Yun, J.; Park, Y.; Yang, S.; Kim, S. Large Voltage Generation of Flexible Thermoelectric Nanocrystal Thin Films by Finger Contact. *Adv. Energy Mater.* **2017**, *7* (21), 1700972.

(12) Gao, J.; Miao, L.; Liu, C.; Wang, X.; Peng, Y.; Wei, X.; Zhou, J.; Chen, Y.; Hashimoto, R.; Asaka, T.; Koumoto, K. A novel glass-fiber-aided cold-press method for fabrication of n-type Ag<sub>2</sub>Te nanowires thermoelectric film on flexible copy-paper substrate. *J. Mater. Chem. A* **2017**, *5* (47), 24740–24748.

(13) Zhou, C.; Dun, C.; Ge, B.; Wang, K.; Shi, Z.; Liu, G.; Carroll, D. L.; Qiao, G. Highly robust and flexible n-type thermoelectric film based on Ag<sub>2</sub>Te nanoshuttle/polyvinylidene fluoride hybrids. *Nano-scale* **2018**, *10* (31), 14830–14834.

(14) Ju, H.; Kim, J. Chemically Exfoliated SnSe Nanosheets and Their SnSe/Poly(3,4-ethylenedioxythiophene):Poly(styrenesulfonate) Composite Films for Polymer Based Thermoelectric Applications. *ACS Nano* **2016**, *10* (6), 5730–5739.

(15) Chen, Y.; He, M.; Liu, B.; Bazan, G. C.; Zhou, J.; Liang, Z. Bendable n-Type Metallic Nanocomposites with Large Thermoelectric Power Factor. *Adv. Mater.* **2017**, *29* (4), 1604752.

(16) Suemori, K.; Hoshino, S.; Kamata, T. Flexible and lightweight thermoelectric generators composed of carbon nanotube-polystyrene composites printed on film substrate. *Appl. Phys. Lett.* **2013**, *103* (15), 153902.

(17) Madan, D.; Chen, A.; Wright, P. K.; Evans, J. W. Printed Se-Doped MA n-Type Bi<sub>2</sub>Te<sub>3</sub> Thick-Film Thermoelectric Generators. *J. Electron. Mater.* **2012**, *41* (6), 1481–1486.

(18) Cao, Z.; Koukharenko, E.; Tudor, M. J.; Torah, R. N.; Beeby, S. P. Flexible screen printed thermoelectric generator with enhanced processes and materials. *Sens. Actuators, A* **2016**, *238*, 196–206.

(19) Shang, H.; Dun, C.; Deng, Y.; Li, T.; Gao, Z.; Xiao, L.; Gu, H.; Singh, D. J.; Ren, Z.; Ding, F. Bi<sub>0.5</sub>Sb<sub>1.5</sub>Te<sub>3</sub>-based films for flexible thermoelectric devices. *J. Mater. Chem. A* **2020**, *8* (8), 4552–4561.

(20) Wang, Y.; Zhu, W.; Deng, Y.; Fu, B.; Zhu, P.; Yu, Y.; Li, J.; Guo, J. Self-powered wearable pressure sensing system for continuous healthcare monitoring enabled by flexible thin-film thermoelectric generator. *Nano Energy* **2020**, *73*, 104773.

(21) Feng, R.; Tang, F.; Zhang, N.; Wang, X. Flexible, High-Power Density, Wearable Thermoelectric Nanogenerator and Self-Powered Temperature Sensor. *ACS Appl. Mater. Interfaces* **2019**, *11* (42), 38616–38624.

(22) Vieira, E. M. F.; Pires, A. L.; Silva, J. P. B.; Magalhães, V. H.; Grilo, J.; Brito, F. P.; Silva, M. F.; Pereira, A. M.; Goncalves, L. M. High-Performance  $\mu$ -Thermoelectric Device Based on Bi<sub>2</sub>Te<sub>3</sub>/

Sb<sub>2</sub>Te<sub>3</sub> p-n Junctions. *ACS Appl. Mater. Interfaces* **2019**, *11* (42), 38946–38954.

(23) Ruan, L.; Zhao, Y.; Chen, Z.; Zeng, W.; Wang, S.; Liang, D.; Zhao, J. A Self-Powered Flexible Thermoelectric Sensor and Its Application on the Basis of the Hollow PEDOT:PSS Fiber. *Polymers* **2020**, *12* (3), 553.

(24) Lu, Y.; Ding, Y.; Qiu, Y.; Cai, K.; Yao, Q.; Song, H.; Tong, L.; He, J.; Chen, L. Good Performance and Flexible PEDOT:PSS/Cu<sub>2</sub>Se Nanowire Thermoelectric Composite Films. *ACS Appl. Mater. Interfaces* **2019**, *11* (13), 12819–12829.

(25) Coates, N. E.; Yee, S. K.; McCulloch, B.; See, K. C.; Majumdar, A.; Segalman, R. A.; Urban, J. J. Effect of Interfacial Properties on Polymer-Nanocrystal Thermoelectric Transport. *Adv. Mater.* **2013**, *25* (11), 1629–1633.

(26) Zhang, B.; Sun, J.; Katz, H. E.; Fang, F.; Opila, R. L. Promising Thermoelectric Properties of Commercial PEDOT:PSS Materials and Their Bi<sub>2</sub>Te<sub>3</sub> Powder Composites. *ACS Appl. Mater. Interfaces* **2010**, *2* (11), 3170–3178.

(27) He, M.; Qiu, F.; Lin, Z. Towards high-performance polymer-based thermoelectric materials. *Energy Environ. Sci.* **2013**, *6* (5), 1352–1361.

(28) Ren, J.; Wang, C.; Zhang, X.; Carey, T.; Chen, K.; Yin, Y.; Torrisi, F. Environmentally-friendly conductive cotton fabric as flexible strain sensor based on hot press reduced graphene oxide. *Carbon* **2017**, *111*, 622–630.

(29) Huang, L.; Huang, Y.; Liang, J.; Wan, X.; Chen, Y. Graphene-based conducting inks for direct inkjet printing of flexible conductive patterns and their applications in electric circuits and chemical sensors. *Nano Res.* **2011**, *4* (7), 675–684.

(30) Aloui, W.; Ltaief, A.; Bouazizi, A. Transparent and conductive multi walled carbon nanotubes flexible electrodes for optoelectronic applications. *Superlattices Microstruct.* **2013**, *64*, 581–589.

(31) Yu, L.; Shearer, C.; Shapter. Recent Development of Carbon Nanotube Transparent Conductive Films. *Chem. Rev.* **2016**, *116* (22), 13413–13453.

(32) Guan, X.; Zheng, G.; Dai, K.; Liu, C.; Yan, X.; Shen, C.; Guo, Z. Carbon Nanotubes-Adsorbed Electrospun PA66 Nanofiber Bundles with Improved Conductivity and Robust Flexibility. *ACS Appl. Mater. Interfaces* **2016**, *8* (22), 14150–14159.

(33) Lan, X.; Wang, T.; Liu, C.; Liu, P.; Xu, J.; Liu, X.; Du, Y.; Jiang, F. A high performance all-organic thermoelectric fiber generator towards promising wearable electron. *Compos. Sci. Technol.* **2019**, *182*, 107767.

(34) Cho, C.; Stevens, B.; Hsu, J. H.; Bureau, R.; Hagen, D. A.; Regev, O.; Yu, C.; Grunlan, J. C. Completely Organic Multilayer Thin Film with Thermoelectric Power Factor Rivaling Inorganic Tellurides. *Adv. Mater.* **2015**, *27* (19), 2996–3001.

(35) Fan, W.; Guo, C.; Chen, G. Flexible films of poly(3,4-ethylenedioxythiophene)/carbon nanotube thermoelectric composites prepared by dynamic 3-phase interfacial electropolymerization and subsequent physical mixing. *J. Mater. Chem. A* **2018**, *6* (26), 12275–12280.

(36) Hong, C. T.; Kang, Y. H.; Ryu, J.; Cho, S. Y.; Jang, K. Spray-printed CNT/P3HT organic thermoelectric films and power generators. *J. Mater. Chem. A* **2015**, *3* (43), 21428–21433.

(37) Jia, F.; Wu, R.; Liu, C.; Lan, J.; Lin, Y.; Yang, X. High Thermoelectric and Flexible PEDOT/SWCNT/BC Nanoporous Films Derived from Aerogels. *ACS Sustainable Chem. Eng.* **2019**, *7* (14), 12591–12600.

(38) Yao, Q.; Chen, L.; Zhang, W.; Liufu, S.; Chen, X. Enhanced Thermoelectric Performance of Single-Walled Carbon Nanotubes/Polyaniline Hybrid Nanocomposites. *ACS Nano* **2010**, *4* (4), 2445–2451.

(39) Toshima, N.; Oshima, K.; Anno, H.; Nishinaka, T.; Ichikawa, S.; Iwata, A.; Shiraiishi, Y. Novel Hybrid Organic Thermoelectric Materials: Three-Component Hybrid Films Consisting of a Nanoparticle Polymer Complex, Carbon Nanotubes, and Vinyl Polymer. *Adv. Mater.* **2015**, *27* (13), 2246–2251.

(40) Choi, J.; Jung, Y.; Dun, C.; Park, K. T.; Gordon, M. P.; Haas, K.; Yuan, P.; Kim, H.; Park, C. R.; Urban, J. J. High-Performance, Wearable Thermoelectric Generator Based on a Highly Aligned Carbon Nanotube Sheet. *ACS Appl. Energy Mater.* **2020**, *3* (1), 1199–1206.

(41) Luo, T.; Pan, K. Flexible Thermoelectric Device Based on Poly(ether-b-amide) and High-Purity Carbon Nanotubes Mixed Bilayer Heterogeneous Films. *ACS Appl. Energy Mater.* **2018**, *1* (5), 1904–1912.

(42) Hewitt, C. A.; Kaiser, A. B.; Roth, S.; Craps, M.; Czerw, R.; Carroll, D. L. Multilayered Carbon Nanotube/Polymer Composite Based Thermoelectric Fabrics. *Nano Lett.* **2012**, *12* (3), 1307–1310.

(43) Zhang, D.; Zhang, K.; Wang, Y.; Wang, Y.; Yang, Y. Thermoelectric effect induced electricity in stretchable graphene-polymer nanocomposites for ultrasensitive self-powered strain sensor system. *Nano Energy* **2019**, *56*, 25–32.

(44) Zhang, D.; Song, Y.; Ping, L.; Xu, S.; Yang, D.; Wang, Y.; Yang, Y. Photo-thermoelectric effect induced electricity in stretchable graphene-polymer nanocomposites for ultrasensitive strain sensing. *Nano Res.* **2019**, *12* (12), 2982–2987.

(45) Lee, T.; Park, K. T.; Ku, B.; Kim, H. Carbon nanotube fibers with enhanced longitudinal carrier mobility for high-performance all-carbon thermoelectric generators. *Nanoscale* **2019**, *11* (36), 16919–16927.

(46) Bharti, M.; Singh, A.; Singh, B. P.; Dhakate, S. R.; Saini, G.; Bhattacharya, S.; Debnath, A. K.; Muthe, K. P.; Aswal, D. K. Free-standing flexible multiwalled carbon nanotubes paper for wearable thermoelectric power generator. *J. Power Sources* **2020**, *449*, 227493.

(47) Vigolo, B.; Pénicaud, A.; Coulon, C.; Sauder, C.; Pailler, R.; Journet, C.; Bernier, P.; Poulin, P. Macroscopic Fibers and Ribbons of Oriented Carbon Nanotubes. *Science* **2000**, *290* (5495), 1331–1334.

(48) Jestin, S.; Poulin, P. Wet Spinning of CNT-based Fibers. In *Nanotube Superfiber Materials*; Schulz, M. J., Shanov, V. N., Yin, Z., Eds.; William Andrew Publishing: Boston, 2014; Chapter 6, pp 167–209.

(49) Ma, P.; Siddiqui, N. A.; Marom, G.; Kim, J. Dispersion and functionalization of carbon nanotubes for polymer-based nanocomposites: A review. *Composites, Part A* **2010**, *41* (10), 1345–1367.

(50) Kim, S. W.; Kim, T.; Kim, Y. S.; Choi, H. S.; Lim, H. J.; Yang, S. J.; Park, C. R. Surface modifications for the effective dispersion of carbon nanotubes in solvents and polymers. *Carbon* **2012**, *50* (1), 3–33.

(51) Lin, Y.; Liu, J.; Wang, X.; Xu, J.; Liu, P.; Nie, G.; Liu, C.; Jiang, F. An integral p-n connected all-graphene fiber boosting wearable thermoelectric energy harvesting. *Compos. Commun.* **2019**, *16*, 79–83.

(52) Kim, Y.; Lund, A.; Noh, H.; Hofmann, A. I.; Craighero, M.; Darabi, S.; Zokaei, S.; Park, J. I.; Yoon, M. H.; Müller, C. Robust PEDOT:PSS Wet-Spun Fibers for Thermoelectric Textiles. *Macromol. Mater. Eng.* **2020**, *305* (3), 1900749.

(53) Kim, J.; Lee, W.; Kang, Y. H.; Cho, S. Y.; Jang, K. Wet-spinning and post-treatment of CNT/PEDOT:PSS composites for use in organic fiber-based thermoelectric generators. *Carbon* **2018**, *133*, 293–299.

(54) Liu, J.; Liu, G.; Xu, J.; Liu, C.; Zhou, W.; Liu, P.; Nie, G.; Duan, X.; Jiang, F. Graphene/Polymer Hybrid Fiber with Enhanced Fracture Elongation for Thermoelectric Energy Harvesting. *ACS Appl. Energy Mater.* **2020**, *3* (7), 6165–6171.

(55) Kim, J.; Mo, J.; Kang, Y. H.; Cho, S. Y.; Jang, K. Thermoelectric fibers from well-dispersed carbon nanotube/poly(vinylidene fluoride) pastes for fiber-based thermoelectric generators. *Nanoscale* **2018**, *10* (42), 19766–19773.

(56) Xu, H.; Guo, Y.; Wu, B.; Hou, C.; Zhang, Q.; Li, Y.; Wang, H. Highly Integrable Thermoelectric Fiber. *ACS Appl. Mater. Interfaces* **2020**, *12* (29), 33297–33304.

(57) Zhang, L.; Yang, B.; Lin, S.; Hua, T.; Tao, X. Predicting performance of fiber thermoelectric generator arrays in wearable electronic applications. *Nano Energy* **2020**, *76*, 105117.